HHS Public Access

Author manuscript

Nat Methods. Author manuscript; available in PMC 2020 September 30.

Published in final edited form as:

Nat Methods. 2020 January ; 17(1): 93–100. doi:10.1038/s41592-019-0620-7.

Isolating live cells after high-throughput, long-term, time-lapse microscopy

Scott Luro[1,*], **Laurent Potvin-Trottier**[1,2], **Burak Okumus**[1,3], **Johan Paulsson**[1,*]

[1]Department of Systems Biology, Harvard Medical School, Boston, MA, USA.

[2]Present address: Department of Biology, Concordia University, Montreal, Québec, Canada.

[3]Present address: Illumina, Foster City, CA, USA.

Abstract

Single-cell genetic screens can be incredibly powerful, but current high-throughput platforms do not track dynamic processes, and even for non-dynamic properties they struggle to separate mutants of interest from phenotypic outliers of the wild-type population. Here we introduce SIFT, single-cell isolation following time-lapse imaging, to address these limitations. After imaging and tracking individual bacteria for tens of consecutive generations under tightly controlled growth conditions, cells of interest are isolated and propagated for downstream analysis, free of contamination and without genetic or physiological perturbations. This platform can characterize tens of thousands of cell lineages per day, making it possible to accurately screen complex phenotypes without the need for barcoding or genetic modifications. We applied SIFT to identify a set of ultraprecise synthetic gene oscillators, with circuit variants spanning a 30-fold range of average periods. This revealed novel design principles in synthetic biology and demonstrated the power of SIFT to reliably screen diverse dynamic phenotypes.

[*]**Correspondence and requests for materials** should be addressed to S.L. or J.P. spl53@cornell.edu; johan_paulsson@hms.harvard.edu.

Author contributions

S.L., L.P.-T., B.O. and J.P. conceived the study. S.L. designed and fabricated the screening chip, constructed and screened the genetic libraries, and performed the data analysis. S.L. and J.P wrote the paper.

Reporting Summary. Further information on research design is available in the Nature Research Reporting Summary linked to this article.

Data availability

The data that support the findings of this study are available from the corresponding authors upon request.

Code availability

ImageJ macros for image segmentation and MATAB scripts for cell tracking and signal processing are available from the corresponding authors upon request.

Competing interests

S.L. and J.P. are listed as inventors on a provisional patent application covering the SIFT technology.

Additional information

Supplementary information is available for this paper at https://doi.org/10.1038/s41592-019-0620-7.

Peer review information Rita Strack was the primary editor on this article and managed its editorial process and peer review in collaboration with the rest of the editorial team.

Genetic screens play a fundamental role in biology by identifying which genes or parts of genes determine phenotypic properties. Their power depends on the size and complexity of the mutant libraries that can be considered, the types of properties that can be measured, the ability to control growth conditions while ensuring spatiotemporal uniformity, and—because many mutations only change the distribution of phenotypes—on how reliably those distributions are sampled for each mutant.

Flow cytometry is the cornerstone of ultrahigh-throughput single-cell screening technologies. However, these methods only provide endpoint snapshots, and therefore offer little information about growth, intracellular dynamics and responses to environmental changes[1]. Furthermore, because each cell is probed only once, cytometers struggle to distinguish genetically stable properties from transient phenotypic heterogeneity[2]. Specifically, because mutants of interest tend to be rare, it is often the case that many hits in cytometry-based screens are false positives arising from phenotypic outliers. Droplet fluidics can in principle allow for time-lapse monitoring[3], but tracking individual growing cells remains problematic, and low-resolution images fail to accurately capture important phenotypic features, such as localization patterns, segregation at division, cell-cycle effects and expression dynamics.

Technologies based on microscopy allow for a wider variety of phenotypes to be quantified and screened, and often at much higher accuracy than even the best imaging flow cytometers[4]. Well-based microscopy assays are frequently employed for libraries of limited size, particularly for structured libraries (that is, where known mutants belong to addressable compartments)[5]. Recognizing the need to expand image-based screens to unstructured pooled libraries, Emanuel et al.[6] recently tagged a pooled library with barcodes that could be detected with fluorescence in situ hybridization (FISH). This powerful method enabled screening based on brief time-lapse imaging with comprehensive genotype-to-phenotype correspondence. Lawson et al.[7] applied similar FISH-based genotyping to cells grown within a continuous culturing device, greatly extending the duration of time-lapse imaging and expanding the range of measurable dynamic phenotypes. For proof of principle, a library of 3 different genotypes was screened, along with demonstration that the screen could be expanded to 64 variants, a substantial improvement over studying a single strain at a time and an important technical advancement. However, both of these screening methodologies require the integration of genetic barcodes into the library, which in turn places limitations on the types of properties that can be considered, since the barcodes must be physically linked to genetic variation of interest. They also do not allow for downstream analysis of individual cells, such as whole-genome sequencing or RNA-Seq profiling, since genotyping requires sample fixation.

Here we present SIFT, single-cell isolation following time-lapse imaging, as a method for isolating live cells after multigenerational time-lapse microscopy (Fig. 1a). We start with what we think has emerged as the most powerful platform for long-term tracking of cell lineages: a microfluidic device, known as the mother machine, in which cells grow and divide within narrow trenches and are fed diffusively by flowing culture medium as progeny are washed away[8]. Such platforms have recently been used to track several thousand cell lineages in parallel, while imaging multiple cells in each lineage every few minutes for

hundreds of consecutive generations, and recording spatial and temporal changes in growth, physiology and various reporters[9–14]. The growth conditions are kept exceptionally uniform across and within lineages to ensure straightforward comparisons[15], and can be changed on timescales of seconds to days to evaluate the same cells as they adjust to different media[16]. This allows for reliable estimation of the full distributions of a wide range of phenotypes associated with each genotype, by sampling those distributions hundreds of times rather than just once (Fig. 1b). We image and track over 16,000 parallel cell lineages per run and enable the retrieval of any individual cell(s) of choice by integrating a series of microfluidic push-down valves[17], flow channels and an optical trap[18–20], allowing precise collection of each cell into a dedicated off-chip bin without contamination and without effects on mutations or growth. By separating the screening process from the subsequent genotyping, our method allows users to take advantage of any independent improvements in microscopy, cell handling or sequencing, and gain the ability to evaluate mutants with single-nucleotide precision across the genome, without the need to prepare screen-specific strains or insert genetic barcodes.

We illustrate the power of this approach by screening for more regular synthetic gene oscillators. Such oscillators have been of great interest in recent years, but many circuits have been much less accurate than their natural counterparts, oscillating only in a fraction of cells and quickly drifting out of phase. Starting with versions of two of the most celebrated synthetic oscillators—the dual-feedback oscillator[21] and the repressilator[9,22], both composed of simple transcriptional regulatory networks—a single round of screening for each was sufficient to transform circuits that barely oscillated into extremely stable and accurate synthetic oscillators. Some circuit variants coherently oscillated for almost 500 generations before accumulating half a period of phase drift. This produced a small battery of precise oscillators over a 30-fold range of average periods. For the repressilator, timing accuracy was counterintuitively achieved by screening for optimal production rates of a fourth and unregulated mutant repressor, which effectively sequestered another repressor in the circuit and rendered it nonfunctional. The results demonstrate key principles of synthetic biology and stochastic cellular processes and showcase the unprecedented screening capabilities of SIFT.

Results

Mother machine engineered for the collection of live cells.

The mother machine device is composed of a series of single-lineage growth chambers fixed perpendicular to a larger lane with flowing growth medium[8]. To achieve clean single-cell isolation, we remodeled the microfluidic design to include a secondary fluidic passage for cell collection (Fig. 2a). The growth and collection lanes were separated by a series of push-down valves[17], which remained closed during time-lapse imaging. It was not until cell retrieval that the collection valves were opened and the cells of interest were transported to the pristine collection lane via optical trapping, traversing a maximum distance of 600 μm in under 15 s (Fig. 2a,b and Supplementary Video 1). Growth trenches within the collection lane may be seeded with cells of interest for further time-lapse characterization under either the same or different medium conditions (Fig. 2a and Supplementary Video 2).

A second set of push-down valves was installed at the inlets and outlets of both growth and collection lanes. Actuation of the valves permitted stringent, bleach-based sterilization of the chip entrances and upstream tubing infrastructure without harming cells harbored within growth trenches (Fig. 2c,d). This sanitation routine prevented the many rogue cells—originating, for example, from pervasive biofilms founded by microbial cultures used during device loading—from diffusing through open collection valves and contaminating the collection lane, or from obstructing optical trapping routes. On-chip closure of the inlets and outlets also completely halted fluid flow, thereby allowing reliable cell transportation at low optical trap powers (less than 15 mW at the specimen) and mitigation of photodamage[18,23].

Isolation of single cells without contamination or physiological perturbations.

To validate that SIFT enables reliable isolation of live cells from the microfluidic device, we conducted a mock screen of a microbial culture comprised of strains with phenotypes easily discernible at the colony scale. Cells constitutively expressing either a yellow, red or cyan fluorescent protein were each diluted to a ratio of 1:100 in a population of unlabeled cells, which were mixed together and loaded into the screening chip. After a few generations, each growth trench contained a single isogenic lineage (Fig. 3a). The mock bacterial library was cultivated and imaged on chip for 24 h to simulate a typical time-lapse characterization run. After phenotyping, the flow-through from the growth lane was plated, representing an estimate of the input population diversity (Fig. 3b, left panel). Following the on-chip cleaning routine, three cells expressing a red fluorescent protein from a single lineage were transported to the collection lane and the output was plated (Fig. 3b, right panel, well no. 1). Three yellow-colored cells were then screened, followed by three cyan-colored cells. The entire screening sequence was then repeated for three new lineages. The multiwell plating demonstrated perfect isolation of three targeted cells (corresponding to three colonies), from six different lineages, without any loss of viability or visible contamination. The extra colony seen in the first cyan-colored collection (Fig. 3b, right panel, well no. 3) was likely due to the isolation of a cell just before division, giving rise to a pair of colonies in close proximity with smaller than average sizes.

To quantify the impact of the screening procedure (including both on-chip cleaning and optical trapping routines) on mutation rates and cell physiology, we sequenced the genomes of clonal populations arising from isolated single cells. From each of the 15 unpooled isolates, we found no unique genomic mutations as compared with non-screened recent ancestors, even with optical trapping times of up to five-fold greater than the maximum transport time used in practice (Fig. 3c). Plasmids of single-cell isolates retrieved from the same lineages with standard trapping durations also did not show any unique mutations (see Methods). Additionally, by relocating cells to empty growth trenches, we observed the instantaneous growth dynamics of cells across a wide range of optical trapping times. It was shown that even transport times that were more than five times greater than those used during typical screens did not substantially elevate doubling times (Fig. 3d) or lead to higher rates of cell death (Supplementary Fig. 1). Together, these controls demonstrate that the SIFT screening procedure can have a negligible impact on the mutation rates and physiology of isolated cells.

Genetic screen rescues oscillations of the dual-feedback circuit without chemical inducers.

We next applied SIFT to the development of synthetic gene oscillators, which exhibit phenotypes difficult to observe and impossible to quantify without long-term time-lapse imaging. We first turned to the dual-feedback oscillator, an elegantly simple design comprised of linked positive and negative transcriptional feedback loops[21] (Fig. 4a). One reported feature of this circuit was the ability to tune the average oscillatory period by changing the concentrations of chemical inducers: arabinose to stimulate the activator, AraC, and isopropyl β-D-1-thiogalactopyranoside (IPTG) to sequester binding of the repressor, LacI. However, without any inducers in the medium, the dual-feedback circuit showed no signs of oscillations (Fig. 4d). We therefore screened for genetically altered circuits capable of sustained regular oscillations, even without supplemented drugs.

To create an assortment of oscillatory phenotypes, we generated a rationally guided genetic library of the dual-feedback circuit. Mutagenesis was targeted to operator sites to vary the binding affinities, as well as to ribosome-binding sites (RBSs) and core promoter elements to modulate expression levels, of both AraC and LacI (Fig. 4a). Additionally, AraC was transformed into a constitutive activator by a single point mutation[24] since the protein cannot function as an activator without arabinose. In total, the genetic library contained up to roughly half a million unique variants.

Time-lapse recordings of the library for longer than 50 *E. coli* generations in the mother machine revealed a rich diversity of phenotypes, with many mutants exhibiting regular oscillations. The average periods ranged from under 15 min for some mutants to over 2 h for others (Fig. 4b,c). The heterogeneity was quantified by the coefficient of variation (CV; the mean-normalized standard deviation) in period and amplitude, and revealed that variants with shorter periods typically exhibited greater regularity in timing (Fig. 4b). Furthermore, library variants with lower amplitude noise generally had lower period noise (Supplementary Fig. 2), as might be expected since variation in peak heights (that is, accumulated green fluorescent protein (GFP) reporter proteins) will inevitably translate to variation in decay times, and therefore oscillatory periods.

We isolated eight variants from the genetic library. All individual cells from each lineage were successfully isolated, and all isolates had the same genetic alterations within lineages but were distinct between lineages (Supplementary Fig. 3). Five of the isolated variants were thoroughly characterized by imaging thousands of mother cells of the same genotype. The most regular oscillator (SL278) had a mean period of 16.8 min, 12.9% CV in the period and an autocorrelation after the first period of 0.5, all in the absence of inducers. This was in stark contrast with the original circuit that exhibited no oscillations without inducers (Fig. 4d and Supplementary Fig. 4). We thus successfully isolated a dual-feedback oscillator variant that not only demonstrated regular timing without supplemented drugs, but even slightly surpassed the oscillatory accuracy of the original circuit with optimized formulations of IPTG and arabinose (Supplementary Fig. 5). The SL278 circuit represents the most regular sub-generational synthetic timer known to date.

Dominant-negative repressilator screen uncovers ultraprecise multigenerational timers.

We then sought to improve the timing of the repressilator, the iconic ring oscillator composed of TetR, LacI and cI (Fig. 5a). Recently, the repressilator was redesigned, guided by principles from stochastic chemistry, to generate synchronous long-term oscillations[9]. One integral feature of the overhaul was the inclusion of a DNA 'sponge' that served to titrate away a set number of TetR proteins. This raised the repression threshold and prevented TetR from entering into the low-copy regime where noise was most pronounced and thereby greatly improved oscillation coherence. However, the theory showed that the placement of the threshold was important: too high thresholds and too low thresholds both increased the overall noise in the circuit. The sponge also relied on decoy TetR binding sites on a high-copy plasmid, which imposed an additional growth burden on cells[25] and was frequently lost (not shown).

We therefore introduced a new protein-based mechanism for TetR titration by expressing a dominant-negative (DN) mutant of TetR, which has compromised DNA-binding activity but still dimerizes[26] (Fig. 5b). The DN TetR should then sequester its wild-type (WT) counterparts in a functionally equivalent manner as the decoy operator sites of the titration sponge, but now TetR repression thresholds were tunable by changing DN TetR expression levels. To explore different thresholds, we generated an expression library of the DN TetR on the backbone of the repressilator circuit and cloned it into *E. coli* lacking ClpXP (Fig. 5a), effectively eliminating protein degradation of the SsrA-tagged repressors[27], and screened the library based on time-lapse imaging.

A rich diversity of oscillatory patterns was revealed in the dominant-negative repressilator library. Average periods ranged from under 2 h to over 7 h, translating to well under 5 generations to over 18 generations (Fig. 5c,d). When protein degradation was introduced to the same repressilator plasmid library, the range of average periods from 50 to 100 min became well covered by regularly oscillating variants (Supplementary Fig. 6). Between the libraries, we identified accurate oscillators that spanned a 15-to 450-min range in mean period with near uniform coverage. Furthermore, as with the dual-feedback library, we observed the expected correlation between amplitude and period noise across dominant-negative repressilator variants (Supplementary Fig. 7). Yet in contrast with the dual-feedback library, repressilators with longer periods generally exhibited better timing (Fig. 5c), a difference well reconciled by stochastic models of each circuit (not shown).

To survey the diversity of the dominant-negative repressilator library, 14 genetic variants were isolated without any contamination between collection groups (Supplementary Fig. 8). The best-performing screened circuit (SL229; ranked by lowest period CV) had a nearly three-fold drop in the period CV to just under 10% (Fig. 5e,f). While this was slightly higher than its estimated period CV of 6.5% during the screen (due to under-sampling oscillations with extremely long periods of nearly 230 min; see Supplementary Fig. 9), the oscillations were still exceptionally regular and exhibited an unprecedented autocorrelation after one period of 0.7 (Fig. 5g), surpassing the accuracy of any known synthetic timer of any period scale to date. Another dominant-negative library isolate (SL224) had a mean period almost twice as long, of 356 min, with a slightly higher period CV of 10.2% (Supplementary Fig. 10). From an alternative perspective of timing regularity, it would take this circuit on average

more than 33 periods (nearly 200 h or roughly 455 generations) to accumulate half a period of phase drift, far surpassing the previous record for the least phase diffusion of a synthetic oscillator at 18 periods[9].

Discussion

Genetic screens at the level of individual cells could be tremendously powerful if it were possible to observe the full distributions of phenotypic properties associated with each genetic makeup and to track the spatiotemporal dynamics of cellular components. This requires an imaging setup in which the same strains are tracked over time, over enough consecutive generations to observe long-term dynamics and, more importantly, to accumulate enough data from each mutant strain such that reliable phenotypic changes can be distinguished from sampling noise. It also requires exceptionally tight control of local growth conditions in order to straightforwardly compare different strains, as well as scalable designs that allow for parallelized imaging.

Here we outfitted a powerful imaging platform—capable of high-throughput, multigenerational, time-lapse imaging under tightly controlled growth conditions—with single-cell screening capabilities. A series of microfluidic valves were engineered for cleaning biofilms, and additional flow channels were added for cell collection in conjunction with an optical trap. The device ensures that any cell can be individually isolated post-imaging without contamination and without genetic or physiological perturbations.

We then applied the SIFT method to identify precise synthetic gene oscillators, a task for which tracking individual cells for many generations is necessary to merely observe the phenotypes of interest, let alone to make quantitative comparisons between circuit variants. Our first screens produced what to our knowledge is the most regular set of synthetic oscillators built so far—keeping phase for tens of periods, or hundreds of generations, without entrainment— with circuits displaying average periods ranging from just over half a generation to almost 20 generations. SIFT thus addresses a critical limiting factor in directed evolution of synthetic network design: accurately and reliably screening complex phenotypes, a step which has lagged far behind library design and construction advancements over the past decade[28,29].

The oscillators uncovered here might also serve as valuable tools in their own right, to help dynamically manipulate protein abundances in cells. For example, our libraries exhibit regular oscillations across a range of oscillatory periods (Supplementary Fig. 6), which could be implemented to probe frequency responses of dynamically encoded cellular signals[30]. The circuits also function without chemical inducers, which is useful in many situations where maintenance of artificial additives is not practical—for example, within the mammalian gut, where oscillators have been deployed to measure bacterial growth rates in vivo[31]—or in situations where such drugs are needed to control other factors.

The screens by SIFT also demonstrated novel design principles for generating precise synthetic timers. For the repressilator, previous work demonstrated that molecular titration via decoy TetR-binding sites was required for regular oscillations[9]. By introducing a protein-

based version of titration—whereby dominant-negative TetR proteins dimerize and sequester WT repressors from binding operator sites—expressed at varying strengths, SIFT revealed repressilator variants with exceptionally regular oscillations. Some mutants even surpassed the accuracy of the original circuit with DNA-mediated titration likely due to optimization of the TetR repression threshold and sharpness of switching[32,33]. This approach to tuning repressor transfer functions by screening protein-based titration strengths could be applied to other oscillators, even via other repressors[34].

That said, the true power of SIFT comes from enabling such a wide range of screening opportunities for complex and long-term dynamics, whether arising from synthetic networks, from long-lived natural states of circadian clocks[35] and bistable switches, or epigenetic factors such as prions[36]. In fact, the method could be equally important for protein engineering. For example, from brief measurements of the activity of an enzyme or a reporter, such as a fluorescent protein (FP), in a single cell, it is hard to know if there is truly an improvement in behavior, or if that individual cell simply produced more of the protein. By observing many copies of the same genotype over long timespans, the true changes in performance are revealed over the noise, while at the same time resolving dynamic properties such as FP maturation delays[37], spatial properties such as oligomerization tendencies[38], or the response of each mutant to changes in growth conditions. Because live individual cells are isolated with SIFT, it is also possible to look beyond single genes, and to, for example, identify any mutation(s) across the genome associated with phenotypes of interest.

Even other cell types, such as yeast[39,40] and non-adherent mammalian cells[41], could be grown and imaged by simple renovation of the microfluidic cell trench dimensions, and optical manipulation of eukaryotic cells has already been demonstrated[18]. Throughput of time-lapse characterization can also be further increased by adding more growth lanes to each device, with time resolution of imaging maintained by microscopy hardware upgrades (for example, TTL-triggered acquisition, larger camera sensors). To increase the throughput of cell retrieval, holographic optical trapping could be implemented to transport more than one cell at a time[42] and washing routines could be automated[43]. We believe the ability to track complex and long-term spatiotemporal dynamics across mutant lineages at high throughput and within controlled environments, combined with the ability to accurately retrieve cells of any kind for downstream analysis without barcoding, could revolutionize genetic screens for a wide range of processes and cell types.

Online content

Any methods, additional references, Nature Research reporting summaries, source data, extended data, supplementary information, acknowledgements, peer review information; details of author contributions and competing interests; and statements of data and code availability are available at https://doi.org/10.1038/s41592-019-0620-7.

Methods

Strain construction.

All strains used in this research are listed in Supplementary Table 1.

The background strain for the dual-feedback library, SL113, was generated by sequential P1 transduction of Keio collection mutants *ΔlacI785::kan* (CGSC 8528) and *ΔaraC771::kan* (CGSC 11760) into NDL162, a motility-deficient (*ΔmotA*) *E. coli* K-12 MG1655 strain harboring constitutive mKate2 expression. The background strain for the dominant-negative repressilator library (without protein degradation by ClpXP), was created by P1 transduction of *ΔclpXP::kan* from DHL678 into SL113. The flippase recognition target (FRT)-flanked kanamycin resistance cassettes were removed with expression of flippase (FLP) recombinase (pCP20) from both library background strains.

Design and assembly of synthetic gene oscillator libraries.

All plasmids and synthetic DNA used in this research are listed in Supplementary Tables 2 and 3, respectively.

Dual-feedback circuit library.—The AraC protein, encoded on pJS167, was made a constitutive activator with the substitution Y13H[24] using 'round-the-horn sitedirected mutagenesis (http://openwetware.org/wiki/%27Round-the-horn_sitedirected_mutagenesis) creating pSL978. Diversity of *araC* expression strength and AraC binding affinity was encoded in PAGE-purified degenerate oligonucleotides (Integrated DNA Technologies (IDT)) with machine-mixed, equal-frequency nucleotides targeted to both the *araI1* (ref. [44]) and *lacO1* (ref. [45]) operator sites as well as the RBS[46]. The regulatory library oligonucleotides were then double-stranded with Q5 polymerase (New England Biolabs (NEB)) and Gibson assembled into pSL978, following linearization with Accuprime polymerase (Invitrogen) and gel-purification (Qiagen). The regulatory library of *lacI* was prepared using the same strategy but with pJS169 as the vector. The two isothermal assembly reactions were then mixed, transformed into JP711 by electroporation, and plated on Luria-Bertani (LB) agar with carbenicillin (25 μg ml^{-1}) and kanamycin (50 μg ml^{-1}) at the maximum density without neighboring colonies in contact. Double transformants were pooled together, plasmid-prepped (Qiagen) and put into SL113 via chemical transformation.

Dominant-negative repressilator library.—An expression library for dominant-negative TetR was generated by amplifying a synthetic double-stranded gene fragment (IDT) encoding TetRΔ9–11—designed with different codon usage than the WT *tetR* of the repressilator on pLPT20—with PAGE-purified degenerate oligonucleotides using Q5 polymerase followed by gel purification. Diversity was targeted with machine-mixed bases to the RBS[46] and coupled to four hand-selected constitutive promoters (http://parts.igem.org/Promoters/Catalog/Anderson), all incorporated at equal frequencies. The vector, pLPT20, was linearized with GoTaq Long PCR (Promega), gel-purified and then Gibson assembled with *tetRΔ9–11* library DNAs. The Gibson assemblies were transformed as above with the exception of using plates with only carbenicillin (25 μg ml^{-1}) selection and the final strain

destination strain as SL134 (or SL113 for the dominant-negative repressilator library with protein degradation).

Microfluidic design.

The SIFT device is a two-layer microfluidic chip made of polydimethylsiloxane (PDMS) bonded to a coverslip. The lower flow layer accommodates cells and growth medium, while the control layer directs pressurized fluid to actuate push-down valves. Each layer is cast from a separate silicon wafer (see below). The flow layer blueprint of each chip contains 16,680 25 × 1.5 μm cell trenches spaced 4 μm apart. Cross-channels bridging growth and collection lanes are 200 × 100 μm and spaced 150 μm apart. Flow layer valve structures were introduced using positive photoresist, required to create rounded features necessary for valve closure[17], in contrast to the square profiles of cell trenches and feeding channels. The control layer was designed with two inputs for independent control of valve compression at all the inlets and outlets of the feeding and collection lanes, as well as the entire series of cross-channels connecting the two lanes. The design layout of the control layer was expanded by 1.36% to accommodate PDMS shrinkage relative to the flow layer[47]. All designs were generated with AutoCAD (Autodesk).

Wafer fabrication.

Wafers were fabricated using standard ultraviolet lithography in a clean room environment (Center for Nanoscale Systems at Harvard University). All designs were transferred from quartz-chrome photomasks (Toppan Photomasks Inc. 4090QZA) to 3-inch silicon wafers (University Wafer, ID 695). For the flow layer wafer, cell trenches were made with SU-8 2002 (MicroChem) at a height of 1.4 μm and feeding lanes with SU-8 2010 at a height of 9 μm. Valve structures were added with positive photoresist, AZ 10XT (AZ Electronic Materials), at a height of 10 μm and rounded by reflow at 130 °C for 5 min. The wafer for the control layer was generated using SU-8 2025 at a height of 80 μm. All UV exposures were done with a mask aligner (Suss MJB4) using mercury i-line light cut by a 360-nm longpass filter (Omega Optical PL-360LP) to enhance the sharpness of SU-8 square cross-sectional profiles. Hard baking was done at 150 °C for 20 min following the deposition of each SU-8 layer. Layer heights were verified with a stylus contact profilometer (Dektak XT). Both wafers were silanized to make them robust to many rounds of PDMS casting.

Chip construction.

The SIFT microfluidic device was fabricated with PDMS using multilayer soft lithography. Sylgard 184 Silicone Elastomer (Dow Corning) was mixed at a 20:1 monomer to curing agent ratio, degassed and spin-coated on the flow wafer at 1,200 r.p.m. for 45 s (Headway Research, Inc.) for a thickness of about 70 μm[43]. For the control layer, Sylgard 184 was prepared at a 5:1 ratio, added on top of the control wafer and degassed. The two castings were then partially cured at 65 °C for 25 min, or until the flow later was solid while remaining sticky to the touch. Control layers for each chip were excised, punched with a 0.75-mm biopsy puncher, cleaned with Scotch tape, aligned with a stereomicroscope to the corresponding flow layer region and fully cured to the flow layer at 65 °C for 4 h. The two-layer chips were excised, inlets and outlets were punched, sonicated in isopropyl alcohol for 30 min and then air dried. Glass coverslips (VWR, 24 × 50 mm, No. 1.5) were sonicated in 1

M potassium hydroxide followed by sonication twice in distilled water and dried at 100 °C for 30 min. The PDMS chips were then plasma-bonded to the cleaned coverslips and baked at 100 °C for 1 h. Quality and integrity of bonding was assessed by flowing pressurized distilled water through both control layer inputs at 10 p.s.i., which should fully close valves, and then at 35 p.s.i. for at least 30 min, to ensure no leakage.

Optical trap setup.

Optical trapping was achieved using a linearly polarized ytterbium laser with a central wavelength of 1,064 nm and beam quality factor (M^2) less than 1.1 (IPG Photonics YLR-10–1064-LP) operated in continuous-wave mode. The 5.2 mm collimated beam was directed through a rotatable half-wave plate fixed in front of a polarizing beamsplitter (Thorlabs VBA05–1064). The laser power was regulated by rotation of the wave plate, diverting excess laser to a beam dump and allowing stable power regulation. A shutter was installed (Thorlabs SHB1T) after the beamsplitter to toggle optical trapping while the laser remained on. The laser was enlarged with a 2× achromatic beam expander (Thorlabs GBE02-C) and then directed through a 1:1 Keplerian telescope made of two convex lenses (Thorlabs LA1131-C) positioned on a rail system such that deviation from the sum of focal distances adjusted positioning of the optical trap in the *z* dimension, enabling straightforward parfocalization of the optical trap. Laser light was elevated via a periscope with two mirrors (Thorlabs BB1-E03) mounted on three-knob kinematic mounts (Newport 9807) and directed through a split epi-illumination port of an Eclipse Ti-E Inverted Microscope (Nikon). The near-IR laser was reflected by a dichroic mirror (Chroma ZT1064rdc-sp), focused through a CFI Apochromat TIRF ×100 objective lens (Nikon) with a numerical aperture (NA) of 1.49, and filtered (Chroma ET750sp-2p8) before reaching an Orca-R2 CCD camera (Hamamatsu). Course alignment of the optical train was achieved using the visible guide beam collinear with the 1,064-nm laser; fine alignment was attained by following detailed guides[48,49]. The trap position within the field-of-view (FOV) was visualized at lower power (10 mW after attenuation by half-wave plate and beamsplitter) by temporarily removing the shortpass emission filter, recorded as a region of interest within ImageJ, and saved for use during cell transportation. Logging beam position coordinates enabled trans-illuminated bright-field imaging during cell transportation with the shortpass emission filter engaged.

Library screening.

Cell loading and inlet cleaning.—Colonies from library plates were scraped together and suspended in MOPS EZ rich defined medium (EZRDM; Teknova M2105) with 0.08% (wt/vol) Pluronic F108 (Sigma-Aldrich 542342) and appropriate antibiotics (kanamycin at 50 μg ml^{-1}; carbenicillin at 25 μg ml^{-1}). Pooled library cultures were briefly grown at 37 °C with 220 r.p.m. shaking for 1 h and then concentrated ten-fold by centrifugation at 3,000 r.c.f. for 5 min. Cross-channel valves were actuated with pressurized water at 30 p.s.i., and the concentrated library culture was pipetted into the growth lanes. Inlet and outlet valves were then actuated to halt capillary-driven flow and accelerate cell trench loading via diffusion. Typically, greater than 95% trenches were populated with at least 1 cell after 45 min. While loading, tubing (US Plastic Corp 56515) was connected to the chip with blunt-end needle connections (McMaster-Carr 75165A678) as described previously[15]. The inlet

was cleaned at a volumetric flow rate of 50 μl min^{-1} with 10% bleach (vol/vol) on-chip for 5 min, 10% ethanol (vol/vol) for 30 min, and EZRDM for 10 min, driven by syringe pumps (New Era NE-300). Rapid switching between solutions was enabled with 3-way pinch valve (Bio-Chem Valve 075P3MP12–01S) located less than 5 cm from the chip. Inlet and outlet valves were opened, and medium was flown to cells at 10 μl min^{-1}, continuing throughout the duration of time-lapse imaging. All growth medium and cleaning solutions (with the exception of bleach dilutions) were purified with 0.2-μm filters.

Time-lapse imaging.—Images were acquired using a Nikon Ti inverted microscope equipped with a temperature-controlled incubator (Okolab), CMOS Zyla 4.2 PLUS camera (Andor), Plan Apo Lambda ×40 air objective lens (NA 0.95; Nikon), motorized XY stage (Nikon) and light engine LED excitation source (Lumencor SpectraX). The microscope was controlled by NIS Elements software (Nikon). Focal drift was regulated by a Perfect Focus System (Nikon). The temperature for all screens was maintained at 37 °C. RFP segmentation markers were imaged with 200-ms exposures, while GFP and YFP reporters were imaged with 150 ms; LEDs were set at maximum intensity for all imaging. The following excitation, dichroic, and emission filters (Chroma) were used: RFP (S568/24, 88100, 88101); GFP (S501/16, 88100, 88101); YFP (ET500/20, 69008, 69008). Images were acquired every 5 min for the dual-feedback library and every 8 min for the dominant-negative repressilator library, all saved in 16-bit TIFF format.

Collection cleaning and single-cell isolation.—Growth medium was switched to MOPS minimal medium (MBM; Teknova M2105 supplemented with 0.2% (vol/vol) glycerol and 0.08% (wt/vol) Pluronic F108) and flown at 10 μl min^{-1} for at least 1 h to reduce cell sizes and facilitate removal from trenches. Concurrently, the collection lane was cleaned by flowing 10% bleach (vol/vol) on-chip for 10 min, distilled water for 45 min and then EZRDM for 10 min, all at a rate of 25 μl min^{-1}. The flow rates of both MBM to the growth lane and EZRDM to the collection lane were reduced to 5 μl min^{-1}. The outlet tubing (10 cm or less in length) was fixed above a 48-well plate such that drops were deposited within only a single well. For each binned collection, the following sequence was performed: input medium flows were halted; collection cross-valves was gradually opened at rate of approximately 10 p.s.i. per second; cell(s) of interest (defined by mean *x*-coordinate position per FOV from time-lapse characterization) were transported from cell trenches to the center of the collection lane (taking between 10 to 15 s) by moving the stage about the fixed optical trap, visualized via transilluminated bright-field; collection valves were closed; inlet and outlet valves were opened; flow to the collection and growth lanes was resumed at 25 μl min^{-1}; fluid flows were halted after 1 min of collection; a new empty well was placed beneath the collection outlet; and the process was repeated for as many binned collections as desired. For all cell-trapping routines, the 1,064-nm laser was operated at 1 W, attenuated to 75 mW following the half-wave plate and beamsplitter, and calculated to be at most 15 mW at the specimen, considering laser intensity fluctuations, overfilling the rear aperture of the objective lens, and partial transmission through the objective lens[50].

Time-lapse image analysis.

The core functions of ImageJ and MATLAB scripts for cell segmentation and tracking were provided by fellow Paulsson lab members (Bakshi, S., Leoncini, E., Baker, C., Canas-Duarte, S., Okumus, B. and Paulsson, J., unpublished data).

Cell segmentation.—Cell segmentation was implemented in ImageJ, an open-source image processing software, as a macro script to sequentially call plugins. Time-series images of the RFP channel from each FOV were opened as individual stacks. Local thresholding based on Niblack methodology generated crude binary masks. Watersheding based on the Euclidean distance map separated touching convex structures. A series of erosions and dilations smoothed objects and removed isolated pixels. Objects were filtered based on area and circularity with empirically derived thresholds. Particle properties were recorded, and the mask coordinates were used to extract pixel values from the signal channels (either GFP or YFP).

Cell tracking.—Cell property lists from ImageJ were imported into MATLAB. Objects were filtered again on the basis of dimensions (major-and minor-axis lengths) and proximity to growth trench patterns stereotyped across all images. Spatial densitybased clustering (DBSCAN) was used to group *x*-coordinates of all object centroids across all time points. The object from each time frame within each cluster (that is, belonging to the same lineage) with the greatest y-coordinate value was defined as the mother cell. Single-cell time-traces were constructed by assembling mother-cell properties over time. Traces missing more than 1% of assembled frames or accumulating greater than 10 pixels (1.6 μm with ×40 objective lens) of *xy*-dimensional drift were discarded. If spatial drift was a systematic issue of the imaging run, a marker of constant intensity over time (for example, piece of debris between PDMS and coverslip) was template matched with all time-frames at a given position in ImageJ (cvTemplateMatch plugin). The relative marker position within the FOV was used to translate all particle positions over all time-frames and across all FOVs in MATLAB.

Time-series analysis.—Mother-cell time-traces from both libraries were automatically cropped just prior to a division that exceeded three times the median division time for the trace. Division times were measured by finding local minima of the cell area as a function of time. This culling filtered most cells that died, filamented or otherwise exhibited severe growth defects. Oscillator reporter signals were assessed in terms of concentration (mean pixel intensity normalized by cell area) and were smoothed with a moving mean (sliding window of five frames for repressilator library and three frames for the dual-feedback library) to buffer against minor segmentation errors and help overcome finite time-sampling. Peaks were called using the findpeaks MATLAB function. The peak prominence threshold was adjusted proportionally to the mean top 5% intensity values for each time-trace with a gain defined after manually reviewing several traces. Similar scaling was used for a minimum distance between peaks to avoid calling a peak twice. For the post-screening characterization of individual oscillators, time-traces with odd growth behaviors, irregular segmentation patterns or plasmid-loss events were discarded by semi-automated data perusal. This was possible because processing time was not urgent (screening did not follow phenotyping) and data could be discarded more stringently (many isogenic clones were

observed). Peak calling parameters were not scaled for each time-trace based on intensity, as done for phenotyping of libraries; criteria were fixed across either all repressilator or all dual-feedback characterizations for fair quantitative comparisons.

Peak-to-peak distances were used to calculate period statistics. Peak prominence—the vertical distance from a peak to a value at which the signal begins to increase again—was used for all measures of amplitude. The autocorrelation function was estimated by averaging autocorrelations of single-cell time-traces as described previously[9]. The average time to reach half a period of phase drift was estimated by randomly sampling from period histograms until half a period of drift accumulated. Drawings were repeated until convergence to a single value was attained. This measure was only used to describe repressilator variants as periods were independent from one another.

Cell isolation controls.

The following experiments were used to validate the single-cell isolation procedure of SIFT, which controlled for contamination and percentage of cells recovered; impact on genomic and plasmid mutation rates; and instantaneous growth rates following cell transport.

Sequential single-cell isolation.—Stationary-phase cultures of *E. coli* K-12 MG1655 constitutively expressing either RFP, YFP, CFP or no fluorescent protein from the chromosome (NDL162, LPT38, LPT37 or NDL93, respectively) were mixed at a ratio of 1:1:1:100 by cell density and loaded into the SIFT microfluidic device. The cells were grown and imaged on-chip under rich conditions for 24 h to mimic standard time-lapse phenotyping. In accordance with the single-cell isolation procedure described above, three cells from an RFP-expressing lineage were isolated together (that is, within the same collection bin), followed by three from a YFP-positive lineage and then three from a CFP-positive lineage. This sequence was repeated once more, in the same order, for three different lineages. All cells were plated on LB agar without antibiotics and grow at 37 °C for 16 h.

Sequencing isolated cells.—A mixture of RFP-expressing *E. coli* (NDL162) diluted into a culture of cells not expressing a fluorescent protein (NDL93) at a ratio of 1:100 were loaded into the SIFT chip. Individual RFP-expressing cells were then isolated into separate collection bins by optical-trap transportation for 15 s (the longest time required for cell transportation to the collection lane from a growth trench), 30 s (twice the standard trapping time) and 75 s (5 times the standard trapping time). The sequence was repeated four additional times, returning to the same lineages for each duration of trapping exposure tested (that is, cells were extracted from only three lineages in total). Genomic DNA was individually prepared (Lucigen MC85200) from the 15 isolates grown in LB without antibiotics. Next-generation sequencing libraries were prepared from DNA of each isolate culture, separately, and sequenced on an Illumina MiSeq with a 2 × 150 bp configuration (Genewiz). Read cleaning, sequence alignment and variant calling were done with snippy, a tool for calling substitutions and insertions/deletions between haploid genomes and sequence reads[51]. Paired reads were mapped to a reference sequence (NC_000913.3).

Variants were called above an allele frequency of 20% on reads with mapping quality phred scores greater than 60 and over locations with coverage greater than 30×.

Plasmid DNA from 29 single-cell isolates from the first 10 lineages of the dominant-negative repressilator screen were Sanger sequenced (Genewiz) to verify short-read whole-genome sequencing results as well as to check for plasmid-borne mutations. SeqMan Pro was used to trim trace files above an average quality score cutoff of 12, and then to compile contigs with the default Classic Assembler parameters. Across more than 200 kb of reads, variants were flagged with quality score thresholds of 20 at the SNP and a minimum neighborhood score of 15, using a neighborhood window of 5 bp[52], and a heterozygous trace peak threshold of 50%. All putative variants were then manually screened for persistent changes across all aligned reads from the same cell isolate.

Growth rates following transport via optical trapping.—*E. coli* (NDL162) were grown and imaged in the SIFT device for 24 h. Inlet and outlet valves were closed, cells were transported via optical trapping for varying times and then reseeded in empty trenches or into trenches that were cleared of cells with optical trapping beforehand. Actual transport times deviated from the targeted 1×, 2×, and 5× the standard transport time—as more rigorously followed in the whole-genome sequencing control (see above)—since the time required for re-seeding cells into new trenches was unpredictable; actual transport times are shown in Fig. 3d. The reseeded cells, along with original lineages (cells remaining after progeny relocation) and lineages without any removed cells, were imaged in the RFP channel (see imaging parameters above) every 5 min for 12 h. Single-cell growth rates were calculated by fitting the cell area as a function of time with a single exponential between divisions. Rates derived from fits with standard errors less than 5% were averaged over each time-trace and converted to generation times ($T_{gen} = \ln(2) / r$, where r is the trace-averaged growth rate). Phenotypes not well characterized by growth rates (for example, cell loss or filamentation events) were tabulated (see Supplementary Fig. 1) by manual inspection of movies.

Supplementary Material

Refer to Web version on PubMed Central for supplementary material.

Acknowledgements

We thank R. Yuan for substantial help designing figure illustrations and S. Bakshi for sharing core image-analysis software and providing technical microscopy guidance. All photolithography was performed at the Center for Nanoscale Systems at Harvard University, a member of the National Nanotechnology Coordinated Infrastructure Network, which is supported by the National Science Foundation under award 1541959. All soft lithography was performed at the Microfluidics/Microfabrication Core Facility at Harvard Medical School. This work was supported by the Defense Advanced Research Projects Agency (HR0011-16-2-0049), National Science Foundation (1615487), and National Institutes of Health (R01GM081563).

References

1. Schmitz J, Noll T. & Grünberger A. Heterogeneity studies of mammalian cells for bioproduction: from tools to application. Trends Biotechnol. 37, 645–660 (2019). [PubMed: 30642642]

2. Daugherty PS, Iverson BL & Georgiou G. Flow cytometric screening of cell-based libraries. J. Immunol. Methods 243, 211–227 (2000). [PubMed: 10986416]
3. Kim HS, Guzman AR, Thapa HR, Devarenne TP & Han A. A droplet microfluidics platform for rapid microalgal growth and oil production analysis. Biotechnol. Bioeng 113, 1691–1701 (2016). [PubMed: 26724784]
4. Han Y, Gu Y, Zhang AC & Lo Y-H Review: imaging technologies for flow cytometry. Lab Chip 16, 4639–4647 (2016). [PubMed: 27830849]
5. Denervaud N. et al. A chemostat array enables the spatio-temporal analysis of the yeast proteome. Proc. Natl. Acad. Sci. USA 110, 15842–15847 (2013). [PubMed: 24019481]
6. Emanuel G, Moffitt JR & Zhuang X. High-throughput, image-based screening of pooled genetic-variant libraries. Nat. Methods 14, 1159–1162 (2017). [PubMed: 29083401]
7. Lawson MJ et al. In situ genotyping of a pooled strain library after characterizing complex phenotypes. Mol. Syst. Biol 13, 947 (2017). [PubMed: 29042431]
8. Wang P. et al. Robust growth of Escherichia coli. Curr. Biol 20, 1099–1103 (2010). [PubMed: 20537537]
9. Potvin-Trottier L, Lord ND, Vinnicombe G. & Paulsson J. Synchronous long-term oscillations in a synthetic gene circuit. Nature 538, 514–517 (2016). [PubMed: 27732583]
10. Park J. et al. Molecular time sharing through dynamic pulsing in single cells. Cell Syst. 6, 216–229 (2018). [PubMed: 29454936]
11. Lugagne J-B et al. Balancing a genetic toggle switch by real-time feedback control and periodic forcing. Nat. Commun 8, 1671 (2017). [PubMed: 29150615]
12. Taheri-Araghi S, Bradde S, Vergassola M. & Jun S. Cell-size control and homeostasis in bacteria. Curr. Biol 25, 385–391 (2015). [PubMed: 25544609]
13. Bergmiller T. et al. Biased partitioning of the multidrug efflux pump AcrAB-TolC underlies long-lived phenotypic heterogeneity. Science 356, 311–315 (2017). [PubMed: 28428424]
14. Robert L. et al. Mutation dynamics and fitness effects followed in single cells. Science 359, 1283–1286 (2018). [PubMed: 29590079]
15. Norman TM, Lord ND, Paulsson J. & Losick R. Memory and modularity in cell-fate decision making. Nature 503, 481–486 (2013). [PubMed: 24256735]
16. Kaiser M. et al. Monitoring single-cell gene regulation under dynamically controllable conditions with integrated microfluidics and software. Nat. Commun 9, 212 (2018). [PubMed: 29335514]
17. Unger MA, Chou HP, Thorsen T, Scherer A. & Quake SR Monolithic microfabricated valves and pumps by multilayer soft lithography. Science 288, 113–116 (2000). [PubMed: 10753110]
18. Ashkin A, Dziedzic JM & Yamane T. Optical trapping and manipulation of single cells using infrared laser beams. Nature 330, 769–771 (1987). [PubMed: 3320757]
19. Wakamoto Y, Umehara S, Matsumura K, Inoue I. & Yasuda K. Development of non-destructive, non-contact single-cell based differential cell assay using on-chip microcultivation and optical tweezers. Sens. Actuators B Chem 96, 693–700 (2003).
20. Probst C, Grünberger A, Wiechert W. & Kohlheyer D. Microfluidic growth chambers with optical tweezers for full spatial single-cell control and analysis of evolving microbes. J. Microbiol. Methods 95, 470–476 (2013). [PubMed: 24041615]
21. Stricker J. et al. A fast, robust and tunable synthetic gene oscillator. Nature 456, 516–519 (2008). [PubMed: 18971928]
22. Elowitz MB & Leibler S. A synthetic oscillatory network of transcriptional regulators. Nature 403, 335–338 (2000). [PubMed: 10659856]
23. Ayano S, Wakamoto Y, Yamashita S. & Yasuda K. Quantitative measurement of damage caused by 1064-nm wavelength optical trapping of Escherichia coli cells using on-chip single cell cultivation system. Biochem. Biophys. Res. Commun 350, 678–684 (2006). [PubMed: 17027921]
24. Dirla S, Chien JY-H & Schleif R. Constitutive mutations in the Escherichia coli AraC protein. J. Bacteriol 191, 2668–2674 (2009). [PubMed: 19218388]
25. Wang Z, Xiang L, Shao J, Wegrzyn A. & Wegrzyn G. Effects of the presence of ColE1 plasmid DNA in Escherichia coli on the host cell metabolism. Microb. Cell Fact 5, 34 (2006). [PubMed: 17112383]

26. Berens C, Altschmied L. & Hillen W. The role of the N terminus in Tet repressor for tet operator binding determined by a mutational analysis. J. Biol. Chem 267, 1945–1952 (1992). [PubMed: 1309804]
27. Farrell CM, Grossman AD & Sauer RT Cytoplasmic degradation of ssrA-tagged proteins. Mol. Microbiol 57, 1750–1761 (2005). [PubMed: 16135238]
28. Schaerli Y. & Isalan M. Building synthetic gene circuits from combinatorial libraries: screening and selection strategies. Mol. Biosyst 9, 1559–1567 (2013). [PubMed: 23340599]
29. Bashor CJ & Collins JJ Understanding biological regulation through synthetic biology. Annu. Rev. Biophys 47, 399–423 (2018). [PubMed: 29547341]
30. Levine JH, Lin Y. & Elowitz MB Functional roles of pulsing in genetic circuits. Science 342, 1193–1200 (2013). [PubMed: 24311681]
31. Riglar DT et al. Bacterial variability in the mammalian gut captured by a single-cell synthetic oscillator. Nat. Commun 10, 4665 (2019). [PubMed: 31604953]
32. Brewster RC et al. The transcription factor titration effect dictates level of gene expression. Cell 156, 1312–1323 (2014). [PubMed: 24612990]
33. Buchler NE & Cross FR Protein sequestration generates a flexible ultrasensitive response in a genetic network. Mol. Syst. Biol 5, 272 (2009). [PubMed: 19455136]
34. Betz JL Cloning and characterization of several dominant-negative and tight-binding mutants of lac repressor. Gene 42, 283–292 (1986). [PubMed: 3732806]
35. Teng S-W, Mukherji S, Moffitt JR, de Buyl S. & O'Shea EK Robust circadian oscillations in growing cyanobacteria require transcriptional feedback. Science 340, 737–740 (2013). [PubMed: 23661759]
36. Yuan AH & Hochschild A. A bacterial global regulator forms a prion. Science 355, 198–201 (2017). [PubMed: 28082594]
37. Balleza E, Kim JM & Cluzel P. Systematic characterization of maturation time of fluorescent proteins in living cells. Nat. Methods 15, 47–51 (2018). [PubMed: 29320486]
38. Landgraf D, Okumus B, Chien P, Baker TA & Paulsson J. Segregation of molecules at cell division reveals native protein localization. Nat. Methods 9, 480–482 (2012). [PubMed: 22484850]
39. Spivey EC, Xhemalce B, Shear JB & Finkelstein IJ 3D-Printed microfluidic microdissector for high-throughput studies of cellular aging. Anal. Chem 86, 7406–7412 (2014). [PubMed: 24992972]
40. Li Y. et al. Multigenerational silencing dynamics control cell aging. Proc. Natl. Acad. Sci. USA 114, 11253–11258 (2017). [PubMed: 29073021]
41. Pearl Mizrahi S, Gefen O, Simon I. & Balaban NQ Persistence to anti-cancer treatments in the stationary to proliferating transition. Cell Cycle 15, 3442–3453 (2016). [PubMed: 27801609]
42. Eriksson E. et al. Optical manipulation and microfluidics for studies of single cell dynamics. J. Opt. A Pure Appl. Opt 9, S113–S121 (2007).
43. Okumus B. et al. Single-cell microscopy of suspension cultures using a microfluidics-assisted cell screening platform. Nat. Protoc 13, 170–194 (2017). [PubMed: 29266097]
44. Lu Y, Flaherty C. & Hendrickson W. AraC protein contacts asymmetric sites in the Escherichia coli araFGH promoter. J. Biol. Chem 267, 24848–24857 (1992). [PubMed: 1447222]
45. Betz JL, Sasmor HM, Buck F, Insley MY & Caruthers MH Base substitution mutants of the lac operator: in vivo and in vitro affinities for lac repressor. Gene 50, 123–132 (1986). [PubMed: 3556322]
46. Espah Borujeni A, Channarasappa AS & Salis HM Translation rate is controlled by coupled trade-offs between site accessibility, selective RNA unfolding and sliding at upstream standby sites. Nucleic Acids Res 42, 2646–2659 (2014). [PubMed: 24234441]
47. Madsen MH, Feidenhans'l NA, Hansen P-E, Garnæs J. & Dirscherl K. Accounting for PDMS shrinkage when replicating structures. J. Micromech. Microeng 24, 127002 (2014).
48. Block SM Construction of Optical Tweezers in Cells: A Laboratory Manual -Vol. II, Sec. 7 (Cold Spring Harbor Laboratory Press, 1997).

49. Lee WM, Reece PJ, Marchington RF, Metzger NK & Dholakia K. Construction and calibration of an optical trap on a fluorescence optical microscope. Nat. Protoc 2, 3226–3238 (2007). [PubMed: 18079723]

50. Neuman KC, Chadd EH, Liou GF, Bergman K. & Block SM Characterization of photodamage to Escherichia coli in optical traps. Biophys. J 77, 2856–2863 (1999). [PubMed: 10545383]

51. Seemann T. Snippy: rapid haploid variant calling and core genome alignment. (2015).

52. Altshuler D. et al. An SNP map of the human genome generated by reduced representation shotgun sequencing. Nature 407, 513–516 (2000). [PubMed: 11029002]

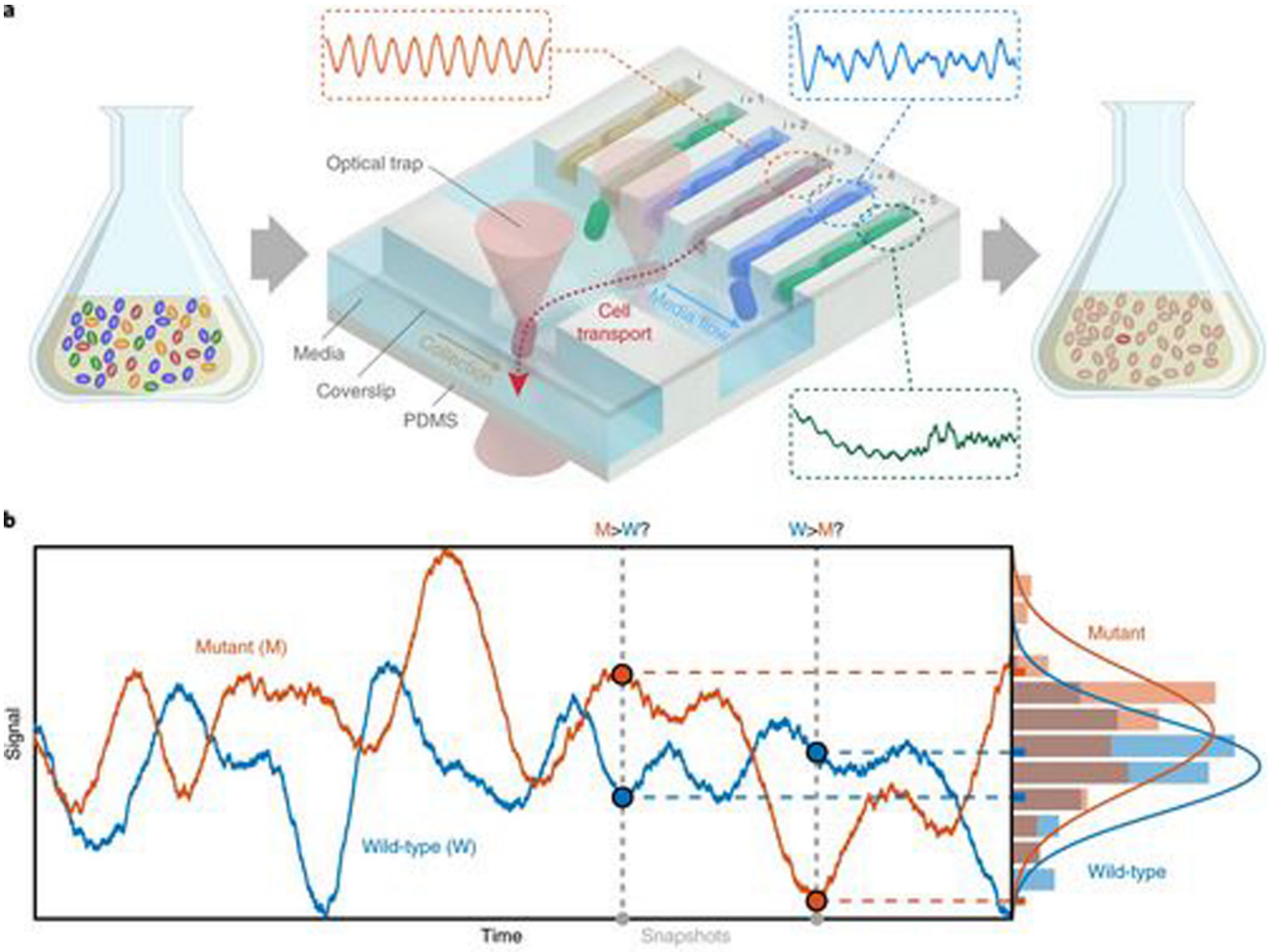

Fig. 1 |. Overview of SIFT.

a, Schematic of the screening process. Any pooled library or complex culture (mixture of colored ovals) can be loaded into the microfluidic device and characterized by long-term time-lapse microscopy. After phenotyping, cells of interest (red cylinders) are transported by optical trapping to a clean area on the chip—previously sterilized with the support of a series of push-down valves—and individually collected from the device without cross-contamination. Isolated cells may be propagated for any downstream off-chip analysis. **b**, A hypothetical example of two different genotypes (represented by generic wild-type (W) and mutant (M) forms) that are frequently mischaracterized by individual single-cell snapshots (colored circles). Only by estimating the full distributions of the phenotypic property (right panel), by assaying the same genotypes over long periods of time (left panel), are the correct classifications reliably assigned.

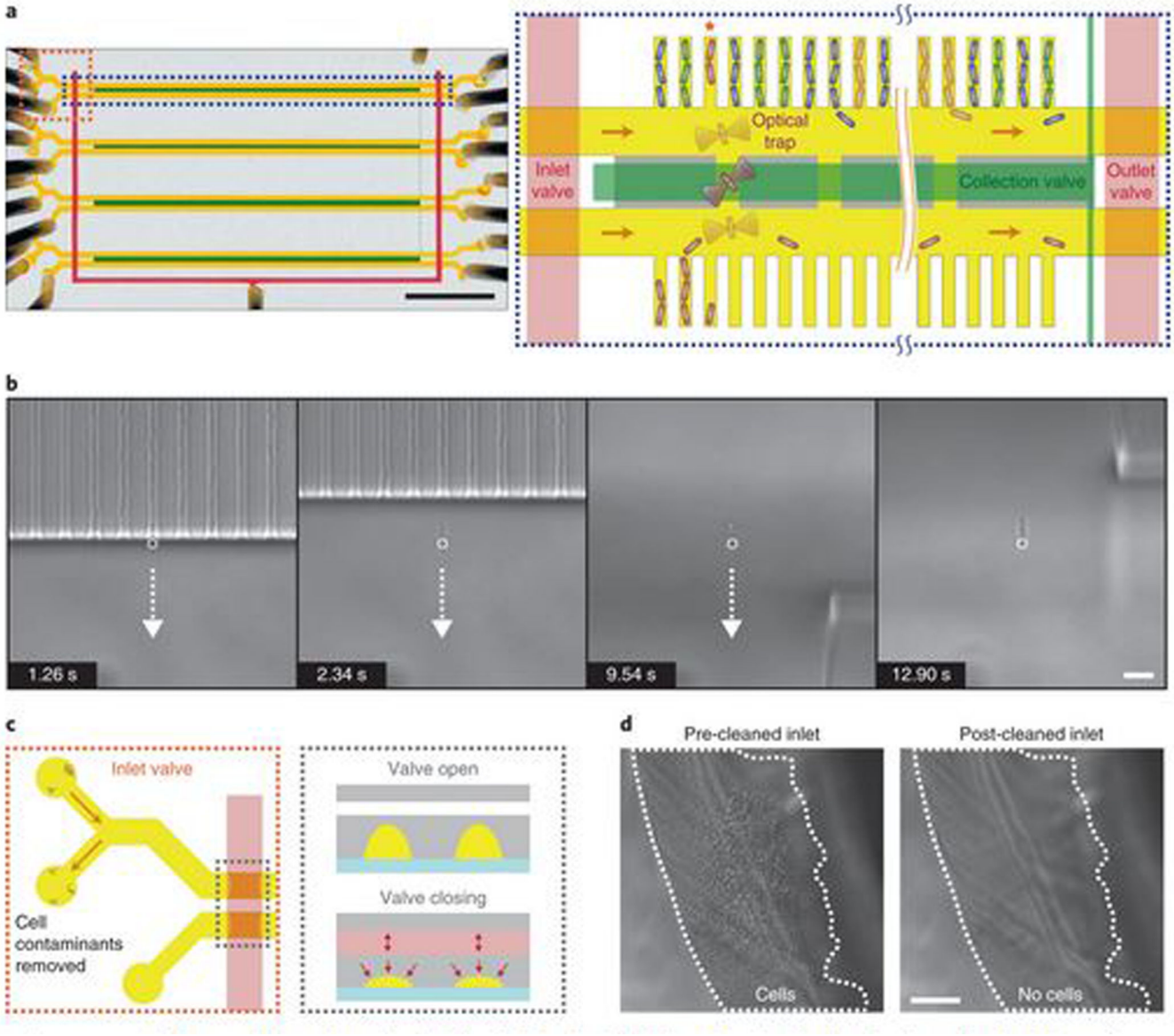

Fig. 2 |. Cell retrieval principles of the SIFT platform.

a, A macroscopic image of the entire microfluidic chip, loaded with dyes for visualization, is shown in the left panel. Dotted boxes correspond to regions represented in other panels. Scale bar, 5 mm. A schematic overview of the single-cell isolation process is shown in the right panel, corresponding to a not-to-scale representation of the blue boxed region from the left panel. Cell(s) from a lineage of interest (marked by red star) are optically trapped and transported to a clean section of the chip—segregated by a series of collection valves (green box)—for further characterization and/or immediate collection. **b**, Kymograph of cell transportation via optical trapping. An *Escherichia coli* cell of interest is removed from a growth trench (leftmost two panels) and dragged through an open collection valve (rightmost two panels) for off-chip collection. White circles mark the optical trap position; dotted arrows indicate the movement direction of the trapped cell. Similar cell transfers were

performed more than 200 times across 5 independent screening runs with similar results. Scale bar, 5 μm. **c**, On-chip inlet-cleaning valve infrastructure. A top-down representation of the entrances for one microfluidic lane (left panel; magnified representation of the orange dotted box from the left panel of **a**) shows deposited bacterial biofilms cleaned by circulated bleach (arrows), while downstream cells residing in growth cavities are protected by a closed push-down valve (red indented box). A cross-sectional view of the push-down valves (right panel; magnified depiction of dotted grey box in the left panel) shows valve actuation. Pressurization of a ceiling chamber causes deflection of a thin PDMS layer that pinches flow channels (yellow) closed. **d**, Images of a feeding lane inlet before (left panel) and after (right panel) biofilm removal by the chip-cleaning procedure outlined in **c**. Similar results were observed across five independent screening runs. Scale bar, 25 μm.

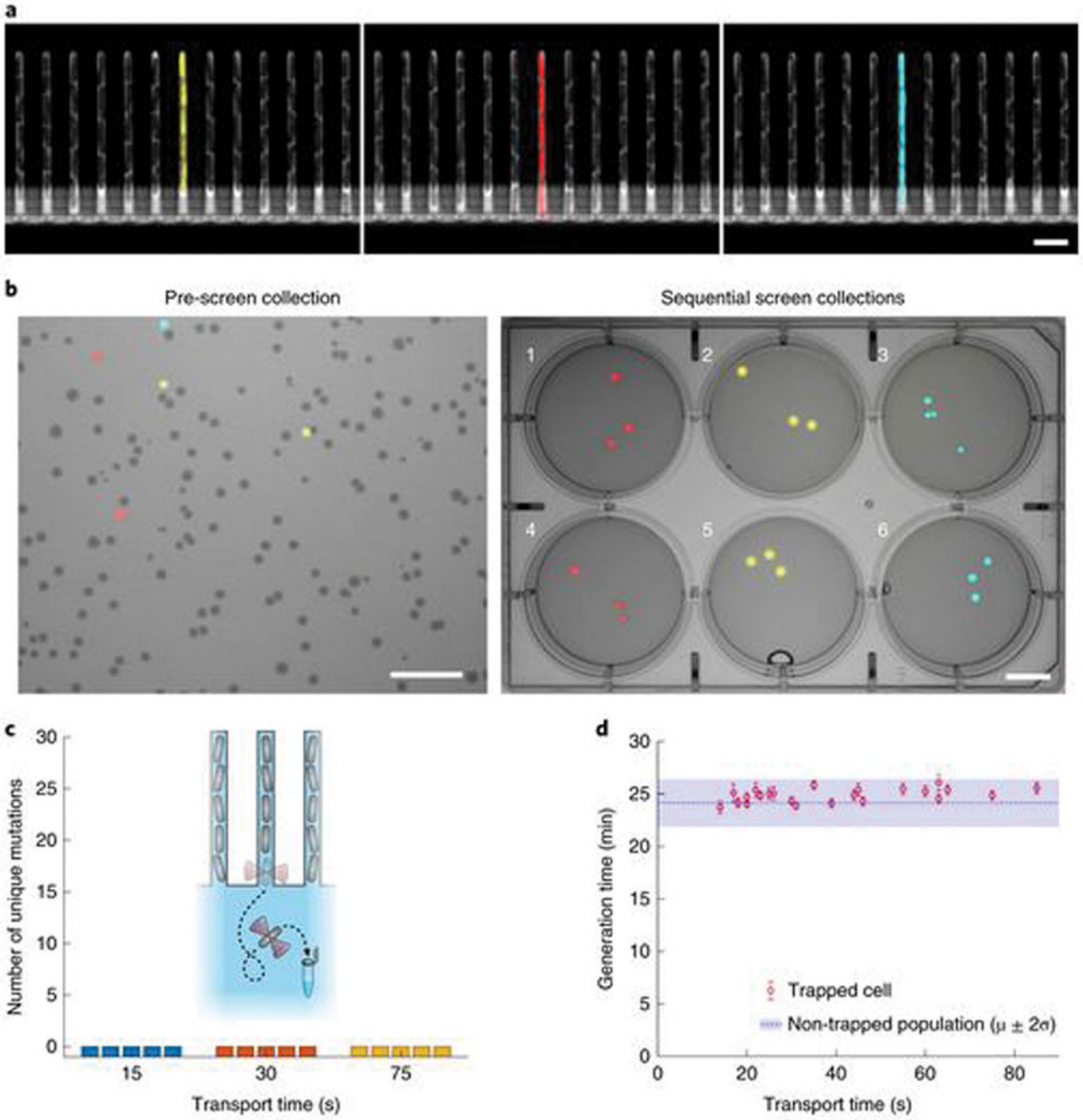

Fig. 3 |. Clean, reliable isolation of live individual cells by SIFT.

a, Sample fields-of-view from the mock color screen comprised of overlaid phase contrast and fluorescence images. *E. coli* were engineered to constitutively express either red, yellow, cyan or no fluorescent protein (rFP, yFP, CFP or no FP), and mixed to a ratio of 1:1:1:100, respectively. Scale bar, 5 μm. **b**, Collection of the chip flow-through prior to SIFT screening the mock library of mixed colored cells (left panel). Three out of three individual cells were isolated from each targeted lineage in the intended sequence. Each agar well is a plating of an independent collection bin; numbers denote the order of collection. Similar results were

observed across three independent mock screening runs. Scale bars, 10 mm. **c**, number of genomic mutations specific to 15 isolated single cells transported via an optical trap for 15 s, 30 s and 75 s (the standard trapping time, two-times longer and five-times longer, respectively). All cells were continuously moved for the entire duration of the respective trapping times to mimic screening transportations, as shown in the schematic. Data were gathered from a single screening run. **d**, Growth-rate-derived generation times immediately following optical transport for varying times, ranging from just over the standard trapping time (15 s) to greater than 5 times longer. Mean generation times (red circles) were measured over a 12-h observation period, with error bars as s.e.m. Mean generation time of 50 non-trapped cells (dotted line; μ) and twice the standard deviation (shaded region; 2σ) represent natural growth heterogeneity within the same experiment. Data were gathered from a single screening run.

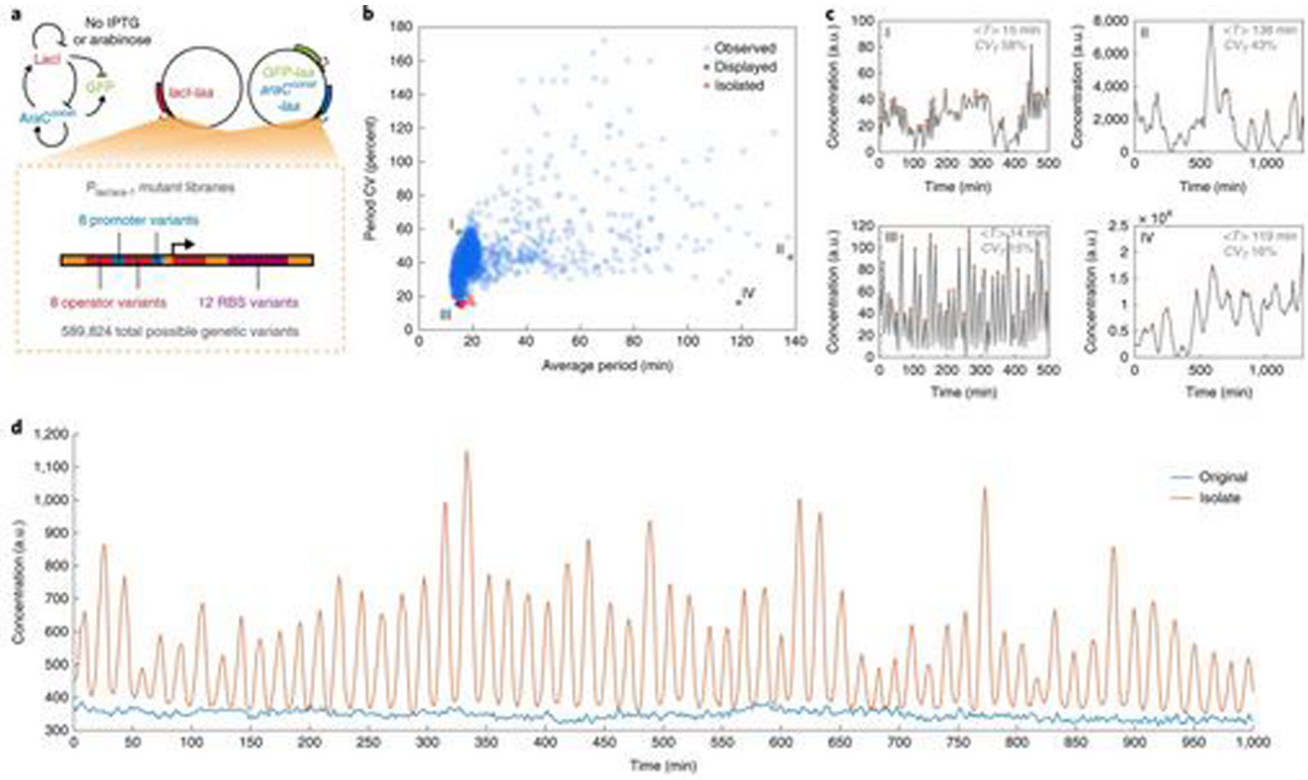

Fig. 4 |. Genetic screen of a dual-feedback oscillator library.

a, The dual-feedback oscillator with linked positive and negative feedback loops (top left panel). All circuit genes, including the GFP reporter, were encoded on two plasmids, transcriptionally regulated by identical $P_{lac/ara-1}$ hybrid promoters, and marked for protein degradation by SsrA (LAA) tags in *E. coli* (top right panel). Library mutations were targeted to promoter, operator and rBS sites of both *lacI* and $araC^{const}$, the *araC* gene with a point mutation (y13H) conferring constitutive activator functionality (bottom panel). **b**, Statistical estimates of period CV and mean period of all library variants with oscillatory-like signals over a 24-h period using SIFT (N_{osc} = 7,803). Variants selected to highlight phenotypic diversity (grey circles with roman numerals) have time-traces shown in **c**. red circles represent variants that were isolated, some of which were individually characterized in a follow-up mother machine run. Mean generation time was 25 min. Library phenotype data were gathered from a single screening run. **c**, Time-traces of selected variants, as described in **b**. Orange dots indicate called peaks. $<T>$, mean period; CV_T, period CV; a.u., arbitrary units. **d**, representative time-traces of the original dual-feedback circuit (SL126) and the best-performing (that is, with the lowest period CV) isolated mutant (SL278), characterized in the mother machine under conditions without any supplemented IPTG or arabinose.

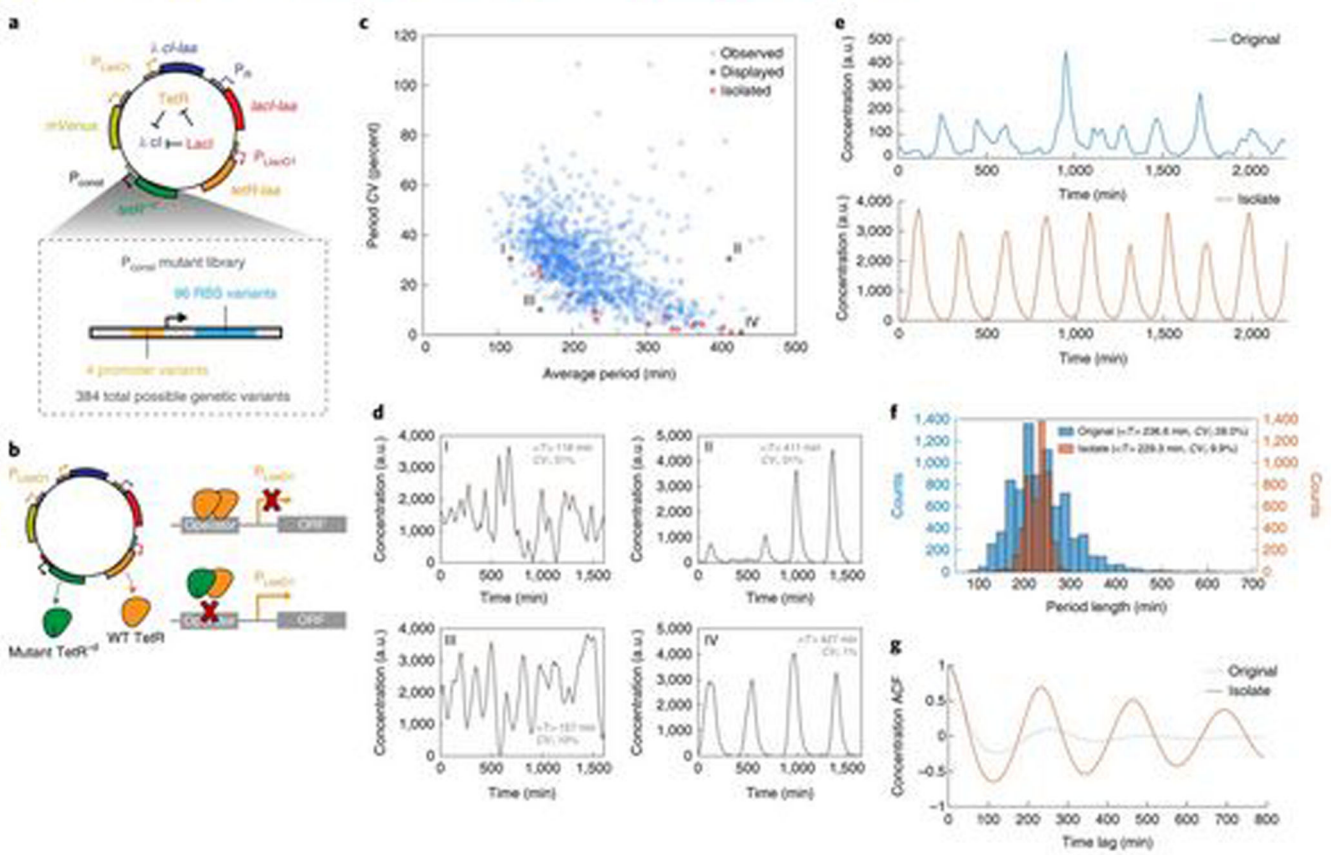

Fig. 5 |. Genetic screen of a dominant-negative repressilator library.

a, An expression library encoding various levels of constitutively expressed (P_{const}) dominant-negative Tetr ($Tetr^{-d}$) was integrated onto the backbone of the repressilator circuit in an *E. coli ΔclpXP* background. **b**, The mutant $Tetr^{-d}$ dimerizes with WT Tetr and prevents binding to cognate operator sites, effectively sequestering a pool of TetR proteins. ORF, open reading frame. **c**, Statistical estimates of period CV and mean period of all library variants with oscillatory-like signals over a 24-hour period using SIFT (N_{osc} = 1,277). Variants selected to highlight phenotypic diversity (grey circles with roman numerals) have time-traces shown in **d**. red circles represent variants that were isolated with SIFT, some of which were individually characterized in a follow-up mother machine run. Mean generation time was 24 min. Library phenotype data were gathered from a single screening run. **d**, Time-traces of selected variants, as described in **c**. Orange dots indicate called peaks. $<T>$, mean period; CV_T, period CV; a.u., arbitrary units. **e**, representative single-cell time-traces of the original repressilator with an integrated reporter (top panel; SL305) and the best-performing (that is, with the lowest characterized period CV) $Tetr^{-d}$ repressilator library isolate (bottom panel; SL229). **f**, Period histograms of the strains from **e**. Histograms include 8,161 periods from the original circuit and 4,779 periods from the top isolate. **g**, Autocorrelation functions (ACF) of strains from **e**.